# Electronic Supporting Information

## Sulfur Incorporation Modulated Absorption Kinetics and Electron Transfer Behavior for Nitrogen Rich Porous Carbon Nanotubes Endows Superior Aqueous Zinc Ion Storage Capability

Jie Li[a]‡, Lai Yu[a]‡, Wentao Wang[b]‡, Xiaoyue He[a], Gongrui Wang[a], Rong Liu[a], Xinyi Ma[a] and Genqiang Zhang[a]*

Ms. J. Li, Mr. L. Yu, Mr. X. Y. He, Mr. G. R. Wang, Ms. R. Liu, Ms. X. Y. Ma, and Prof. G. Q. Zhang

Hefei National Laboratory for Physical Sciences at the Microscale, CAS Key Laboratory of Materials for Energy Conversion, Department of Materials Science and Engineering, University of Science and Technology of China, Hefei, Anhui 230026 China;

Dr. W. T. Wang

Guizhou Provincial Key Laboratory of Computational Nano-Material Science, Guizhou Education University, Guiyang 550018, China

*To whom the correspondence should be referred. Email:gqzhangmse@ustc.edu.cn.

‡ These authors contribute equally to this work.

## 1. Experimental section

### *1.1. Synthesis of SN-PCNTs*

The $MnO_2$ nanofibers were synthesized according to our previous work.[1] In a typical synthesis, 3 mmol of manganese sulfate monohydrate ($MnSO_4 \cdot H_2O$), 2mmol of potassium permanganate ($KMnO_4$) and 2 mmol of ammonium fluoride ($NH_4F$) were dissolved in 40 mL of deionized water, respectively. Then, the above solution was transferred to a 50 mL Teflon-lined autoclave and kept at 150 ºC for 12 h. After cooling down to room temperature, the precipitate was centrifuged and washed with deionized water and ethanol several times. The product of $MnO_2$ nanofibers were obtained by drying in a vacuum at 70 °C overnight. Subsequently, 0.38 mL of pyrrole monomers and 0.29 mL of aniline monomers were dissolved in 50 mL of 0.1 M $H_2SO_4$ solution. Then $MnO_2$ nanofibers (100 mg) in 50 mL deionized water were added into the homogeneous mixture solution with stirring for 4 h under inert atmosphere. The precipitate (denoted as PPy/PANI-NTs) was washed with deionized water and ethanol, respectively, and then dried at 70 °C overnight. The obtained PPy/PANI-NTs were uniformly mixed with sublimed sulfur (the weight ratio 1:2) in a mortar, and then they were calcinated at 600 °C for 2 h in tubular furnace with a temperature increase rate of 2 °C $min^{-1}$ under argon atmosphere to form the final product of S/N codoped porous carbon nanotubes (denoted as SN-PCNTs). In order to investigate the optimal ratio, the different weight ratios between PPy/PANI-NTs and sulfur powder (1:1 and 1:3) also were mixed to synthesize carbon materials. In addition, the PPy/PANI-NTs were directly calcinated at same condition without adding sulfur power to obtain the sample N-PCNTs.

### *1.2. Characterizations*

The morphologies and microstructures of samples were observed by field-emission scanning electron microscopy (FESEM, SU-8220), and transmission electron microscopy (Hitachi HT7700, JOEL, JEM-2010; Talos F200X). Powder X-ray diffraction (XRD) data were collected on a Bruker D8 Advance X-Ray Diffractometer. The Raman spectrum were collected on a Raman spectrometer (Renishaw inVia) with an excitation wavelength of 532 nm. The structural information of the synthesized materials were analyzed by Fourier transform infrared spectroscopy (FTIR, Nicolet 8700, America). The specific surface area and pore size distribution of the electrode materials were measured by Brunauer-Emmett-Teller (BET;

Tristar II 3020M). The surface structure and chemical states of materials were investigated by X-ray photoelectron spectroscopy (XPS, ESCALAB 250, USA),

### *1.3. Electrochemical measurements*

CR2016 coin-type cells were assembled to evaluate the electrochemical measurements of the synthesized materials. The electrodes were prepared by mixing the active materials, carbon black (Super-P) and polytetrafluoroethylene preparation (PTFE) binder (the weight ratio 8:1:1) with a mixed solution ethanol and N-methyl-2-pyrrolidinone (NMP) solvent, then the slurry was coated on graphite paper and dried in a vacuum oven overnight at 80 °C. The mass loadings of the active materials were 1.0-1.5 mg. According to the previous report, the In@Zn counter electrodes were formed by immersing the bare Zn foils in 0.5 M $InCl_3$ aqueous solutions for 10 minutes.[2] Whatman glass microfiber filters (GF/F) as the separator and 2 M $ZnSO_4$ as the electrolyte. The working voltage windows were from 0.2 to 1.8 V. Galvanostatic charge/discharge measurements were performed on a Neware multichannel battery test system. Cyclic voltammetry (CV) and electrochemical impedance spectroscopy (EIS) were obtained using a Four-channel potentiostat CS3104 (Wuhan CorrTest Instruments Corp., Ltd.).

The energy density ($E$, Wh $kg^{-1}$) and power density ($P$, W $kg^{-1}$) of the ZHCs were calculated based on the mass of cathode material according to the following equations:

$$E = I\int Vdt/3.6m \quad (1)$$

$$P = E/\Delta t \quad (2)$$

Where $i$ is the current density, $V$ is the voltage window, $m$ is the mass of active material in cathode and $\Delta t$ is the discharge time.

### *1.4. In-situ Raman experiment*

The in-situ Raman experiment were performed using an in-situ battery (LIB-RAMAN, Beijing Scistar Technology Co., Ltd) in a Raman spectrometer (Renishaw inVia) with a laser excitation at 532 nm. The in-situ battery was fabricated using active material as cathode, In@Zn foil as counter electrode, Whatman glass microfiber filters as the separator, and 2 M $ZnSO_4$ as electrolyte. The charge-discharge profile was carried out in the voltage window of 0.2-1.8 V using a Neware BTS-610 battery tester.

### *1.5. Computational details*

The density functional theory (DFT) calculations were implemented by the Vienna Ab-initio Simulation Package (VASP)[3, 4] with the projected augmented wave (PAW) method [5]. The kinetic cutoff energy with the plane wave basis set is 500 eV. The geometric optimizations and electronic structure were calculated by using the Perdew-Burke-Ernzerhof (PBE) exchange-correlation potential within the generalized gradient approximation (GGA), and they were entirely relaxed with the convergence criteria of energy and force set at $10^{-4}$ eV and 0.03 eV $Å^{-1}$.[6] Bader charge calculations were further applied to analyze the charge transfer between Zn and SN-PCNTs. The charge density difference quantifies the redistribution of electron charge due to Zn and graphene fragment interaction. The Monkhorst-Pack[7] K point mesh size with gamma point was selected for the graphene fragment's irreducible first Brillouin zone integrations. The pyridinic-N, pyrrolic-N and graphite-N[8] atoms doped graphene fragment to the model N-PCNTs, while in this N-PCNTs, the S atom substitutes one of the graphene C to the model SN-PCNTs. The adsorption energy ($E_{ads}$) was calculated using the following equation:

$$E_{ads} = E_{total} - E_{fragment} - E_{Zn} \quad (3)$$

Where $E_{total}$ and $E_{fragment}$ were the total energy after and before the introduction of Zn ion, respectively. $E_{Zn}$ is the energy of the Zn atoms.

## 2. Characterization

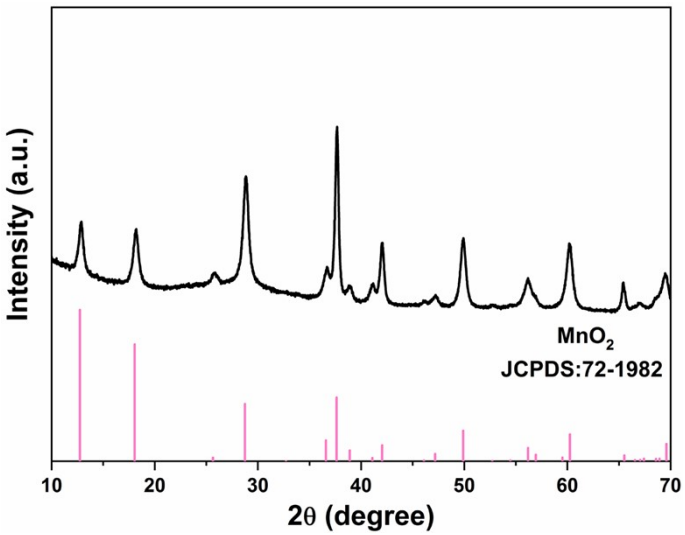


**Fig. S1** The XRD pattern of $MnO_2$ nanowires.

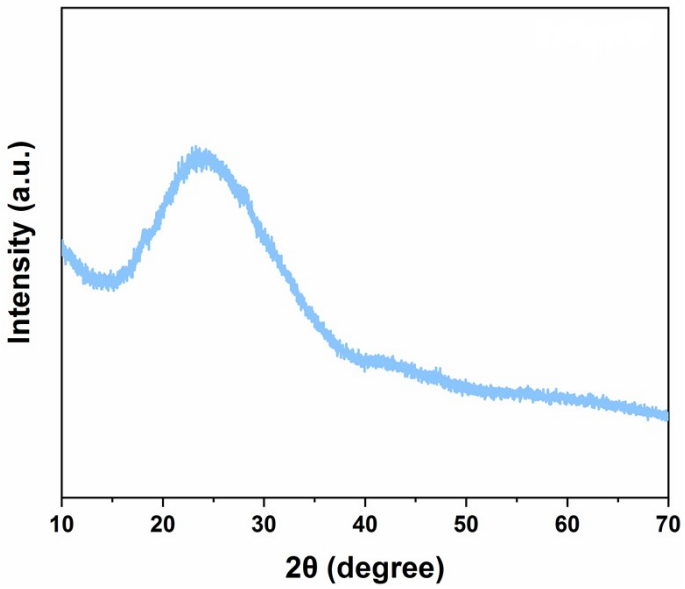


**Fig. S2** The XRD pattern of PPy/PANI-NTs precursor.

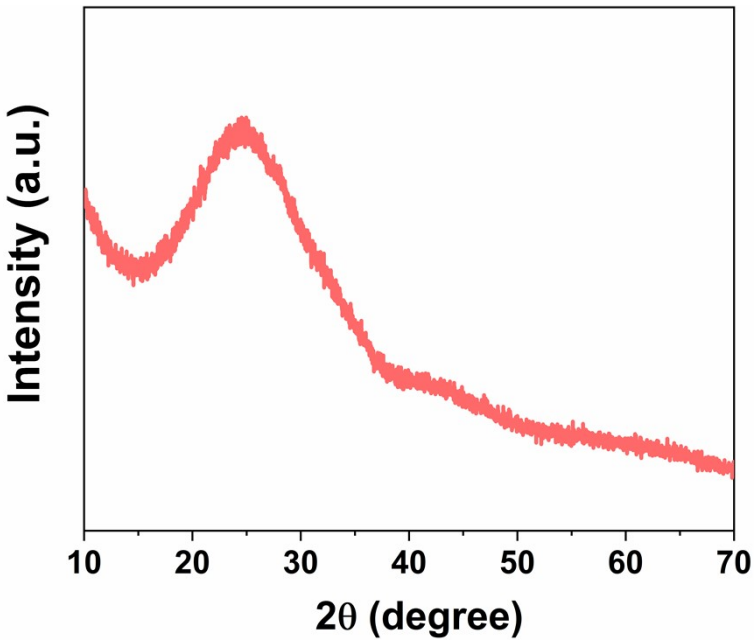


**Fig. S3** The XRD pattern of SN-PCNTs.

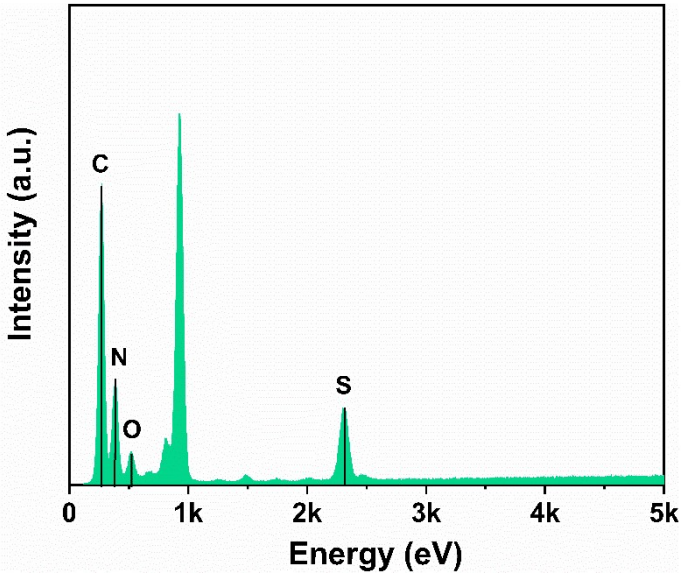


**Fig. S4** The EDX spectrum of SN-PCNTs.

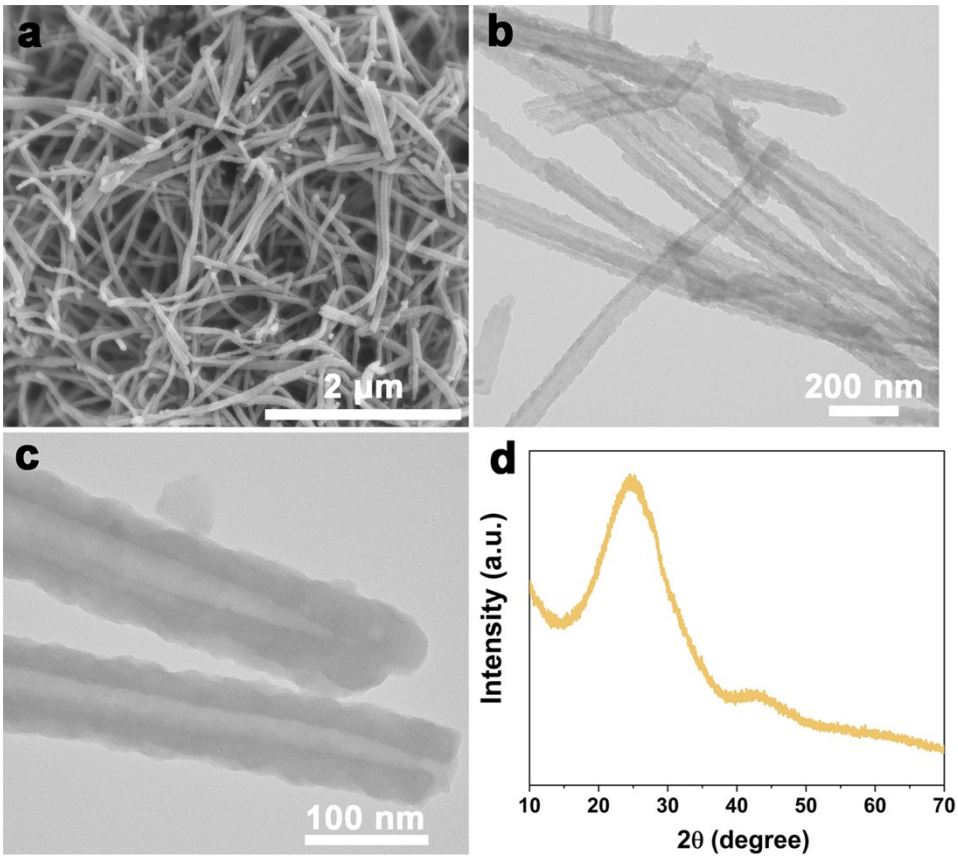


**Fig. S5** The (a) SEM, (b,c) TEM images and (d) XRD pattern of N-PCNTs.

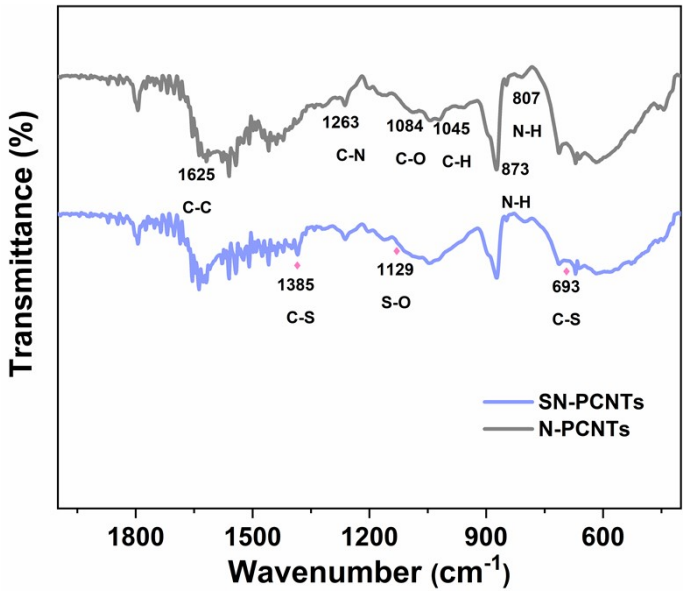

**Fig. S6** The FTIR spectra of SN-PCNTs and N-PCNTs.

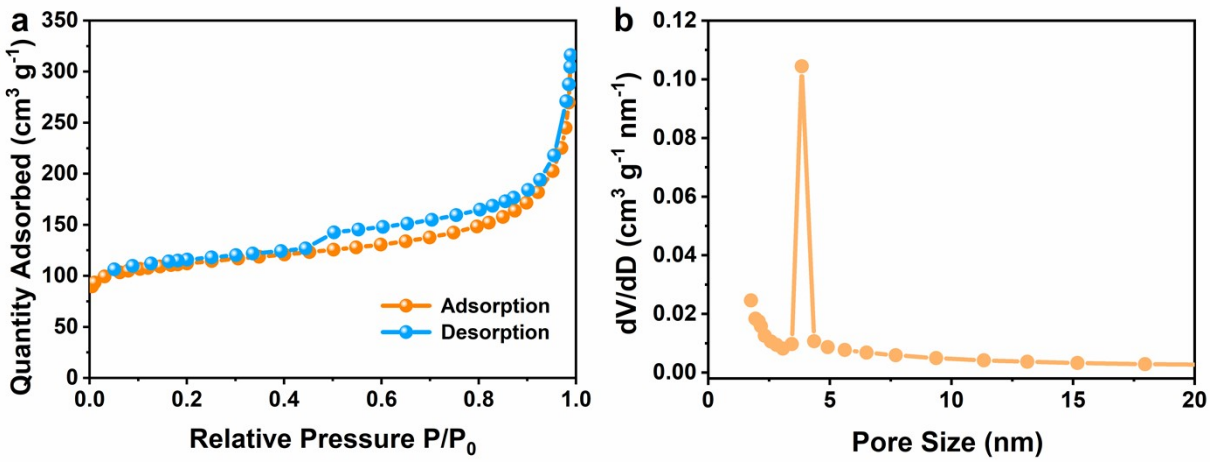


**Fig. S7** (a) $N_2$ adsorption-desorption isotherm and (b) corresponding pore size distribution of N-PCNTs.

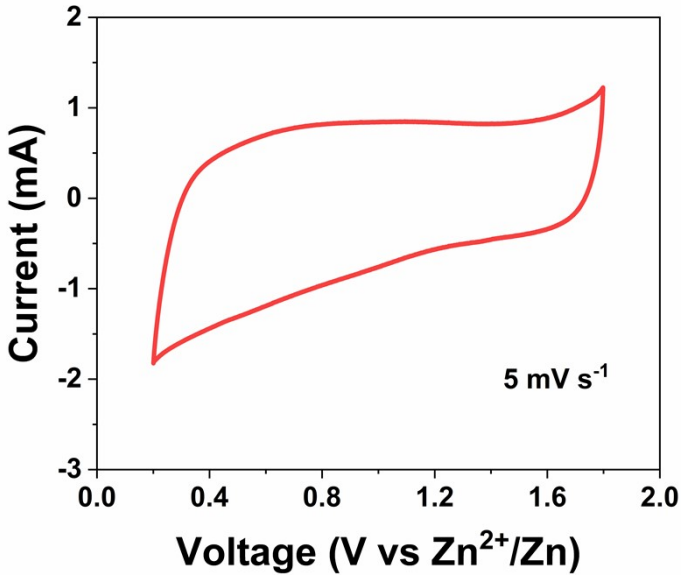


**Fig. S8** The CV of SN-PCNTs at 5 mV s$^{-1}$.

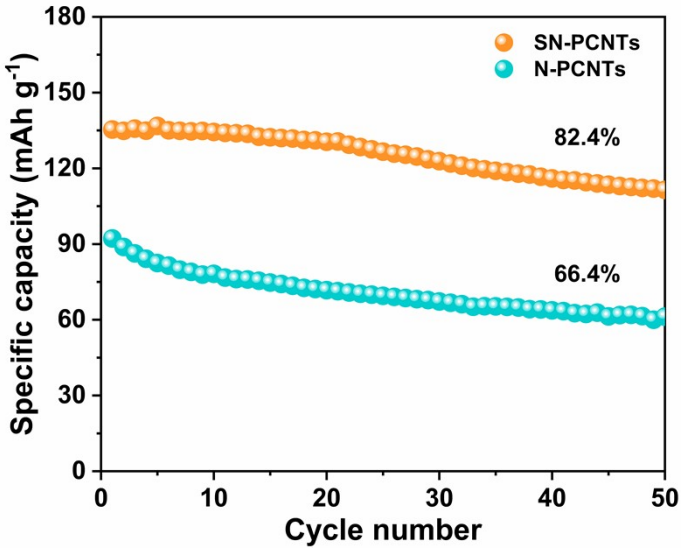


**Fig. S9** Cycling performance of SN-PCNTs and N-PCNTs cathodes at 0.5 A $g^{-1}$.

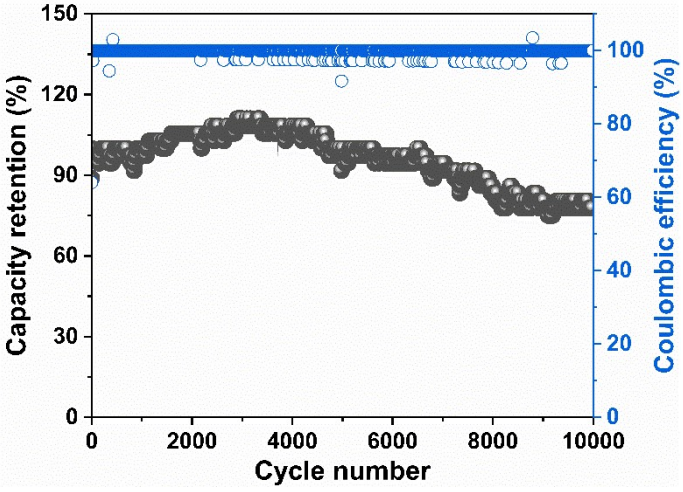


**Fig. S10** Cycling stability and coulombic efficiency of N-PCNTs electrode at 5 A $g^{-1}$.

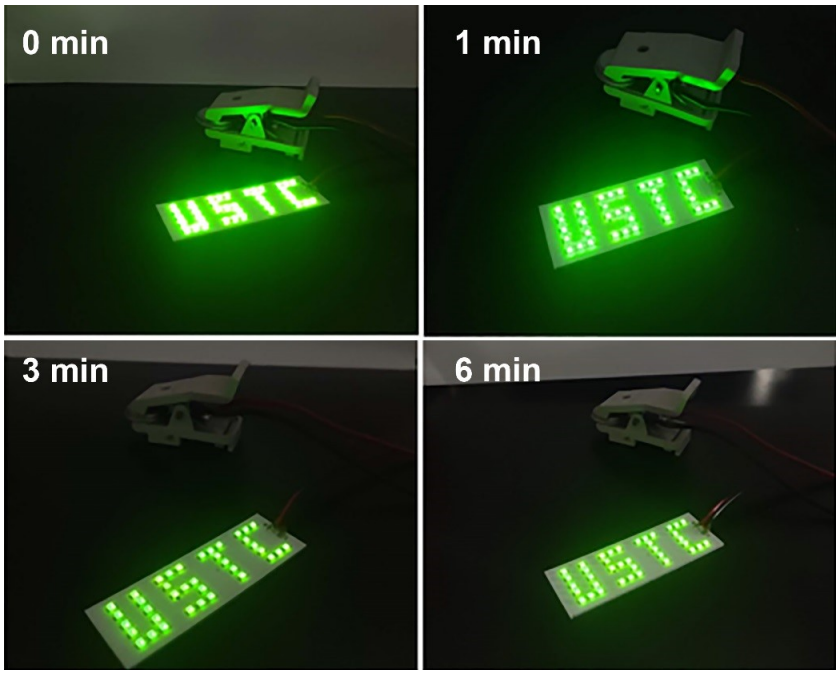


**Fig. S11** Photograph of the LEDs lamps powered by two SN-PCNTs-based ZHCs at different discharge times.

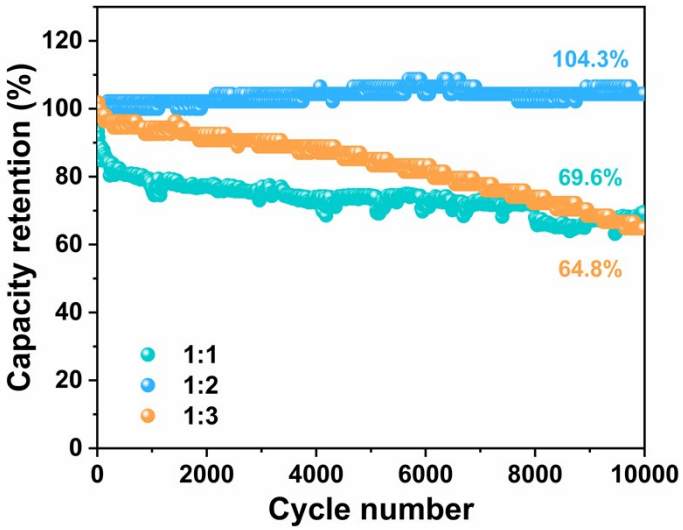


**Fig. S12** Cycling performance of the SN-PCNTs cathodes with different mass ratios (PPy/PANI-NTs: Sulfur) at 5 A $g^{-1}$.

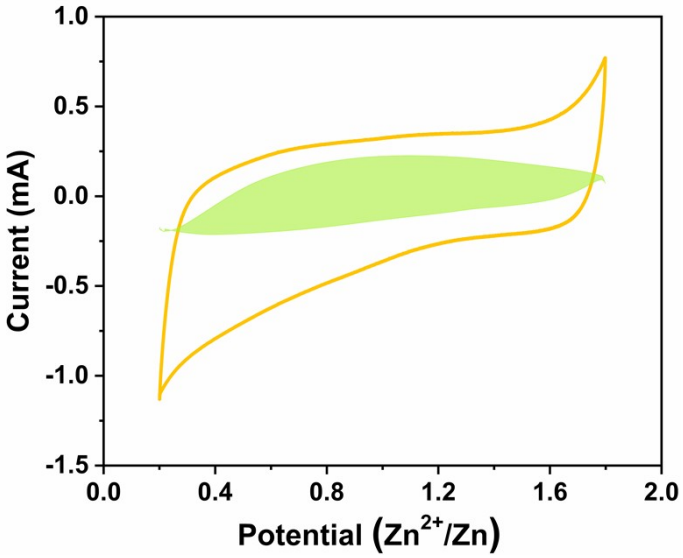


**Fig. S13** Capacitive-controlled contribution of SN-PCNTs at 2 mV $s^{-1}$.

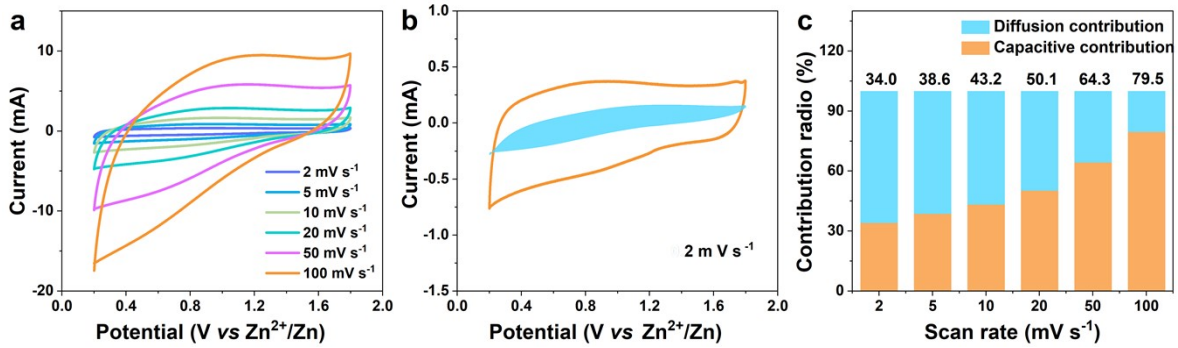


**Fig. S14** (a) The CV curves of N-PCNTs cathode at different scan rates. (b) Contribution of capacitive-controlled process in the N-PCNTs at 2 mV $s^{-1}$. (c) Contribution ratio of the capacitive- and diffusion-controlled process in the N-PCNTs cathode at different scan rates.

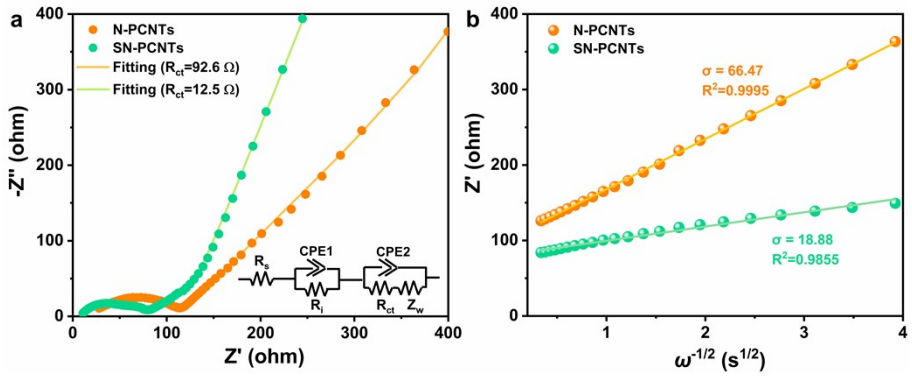


**Fig. S15** (a) Nyquist impedance plots of N-PCNTs and SN-PCNTs electrodes, and the inset shows equivalent circuit model. (b) Linear fitting to Z' versus $\omega^{-1/2}$ plots in the low frequency range.

The diffusion coefficient of $Zn^{2+}$ can be calculated according to the equation:[9]

$$D=R^2T^2/2n^4A^2F^4c^2\sigma^2 \quad (4)$$

Where *R*, *T*, *n*, *A* and *F* represent the gas constant, absolute temperature, electron number, area of the electrode, and Faraday constant, respectively. The *c* is the electrolyte concentration, $\sigma$ is the slope of *Z'* and $\omega^{-1/2}$ in low-frequency region. Therefore, the calculated $Zn^{2+}$ diffusion coefficients of SN-PCNTs and N-PCNTs are $1.21 \times 10^{-12}$ and $9.78 \times 10^{-14}$ $cm^2\ s^{-1}$, respectively.

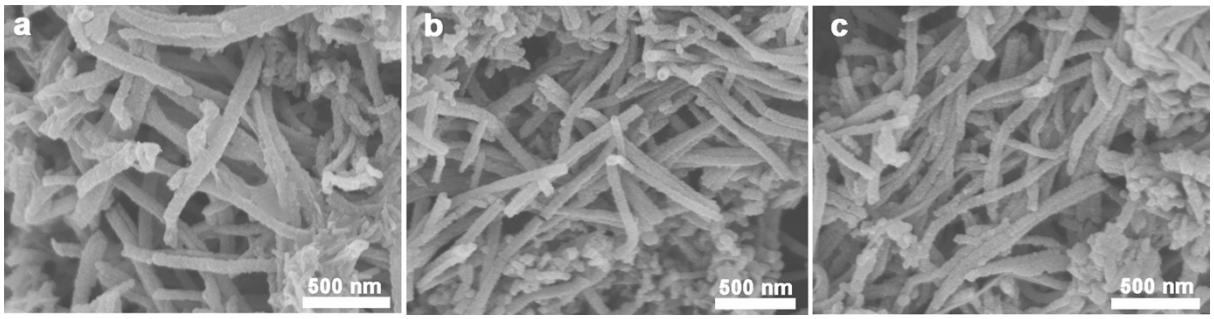


**Fig. S16** The ex situ SEM images of SN-PCNTs cathode at (a) stage A, (b) stage C and (c) stage E.

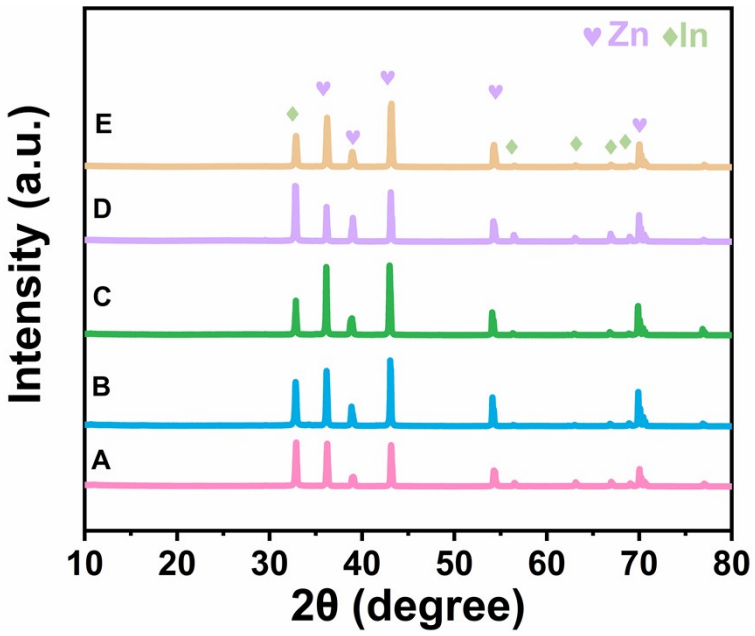


**Fig. S17** The ex situ patterns of In@Zn electrodes.

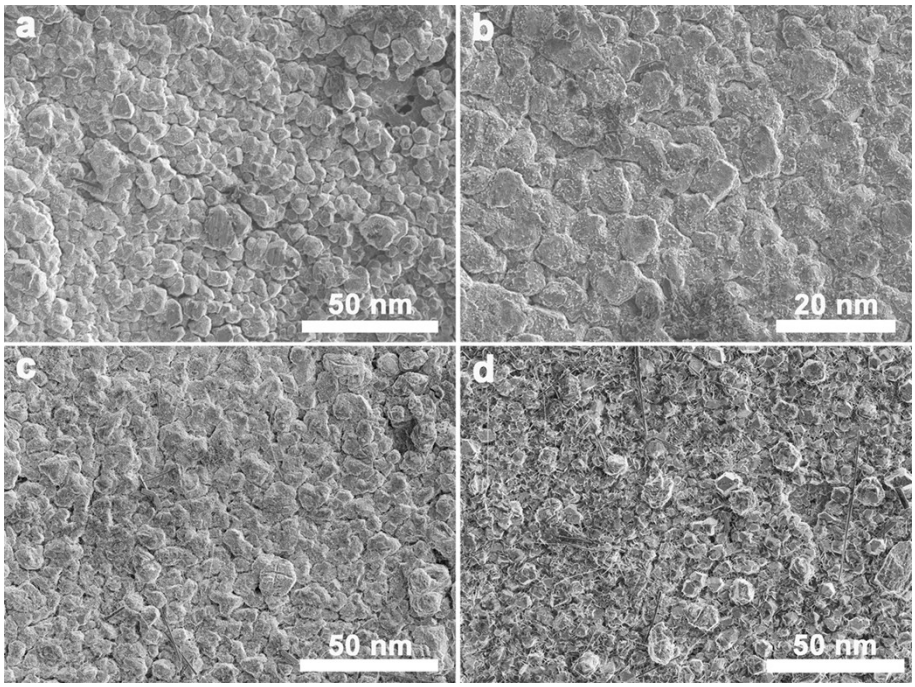


**Fig. S18** (a) The SEM image of fresh In@Zn anode. Ex situ SEM images of In@Zn anodes at (b) stage A, (c) stage C and (d) stage E.

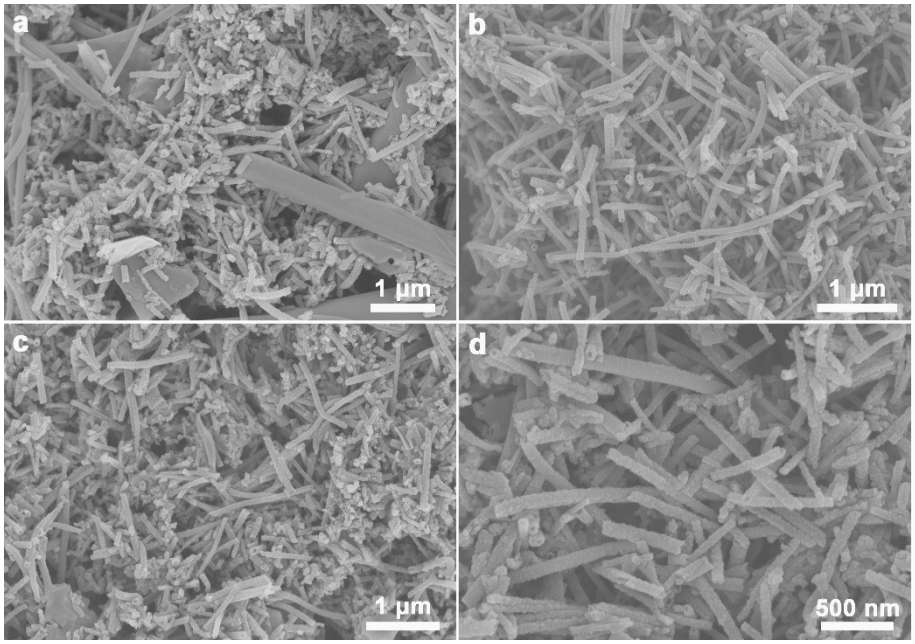


**Fig. S19** SEM images of (a) N-PCNTs and (b) SN-PCNTs electrodes after 10000 cycles at 5 A $g^{-1}$; (c, d) SEM images of SN-PCNTs cathode after 25000 cycles at 5 A $g^{-1}$.

As shown in Fig. S19, the nanotube morphology of N-PCNTs was disrupted, while the SN-PCNTs cathode could be well retained after long-term cycling over 10000 cycles at 5 A $g^{-1}$, which is one of the reasons for the better cycling performance of SN-PCNTs. Furthermore, even after 25000 cycles, the morphology of SN-PCNTs electrode was only slightly damaged.

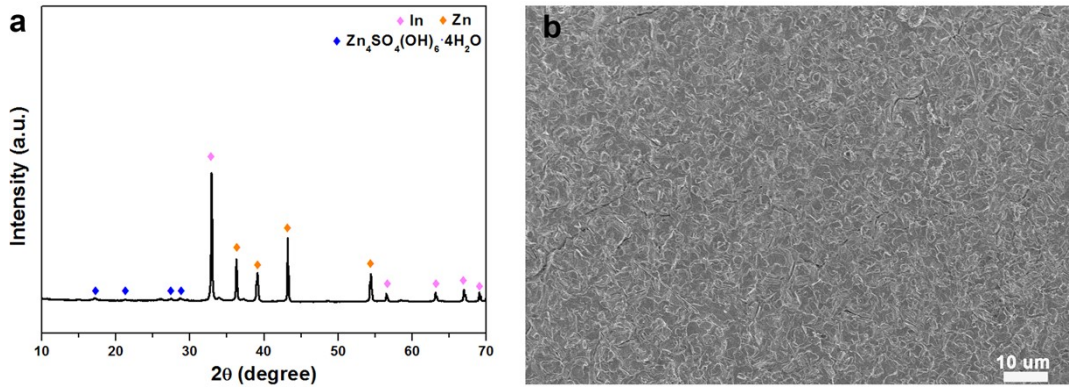


**Fig. S20** (a) The XRD pattern and (b) SEM image of In@Zn anode after 4000 cycles at 5 A $g^{-1}$.

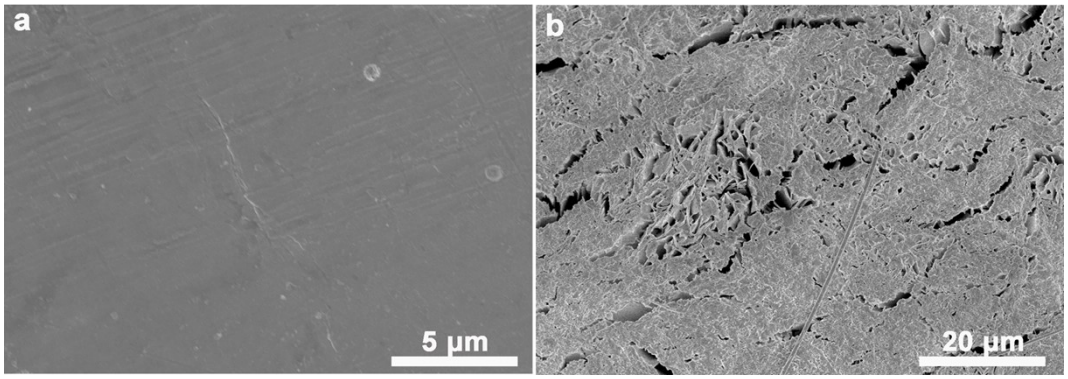


**Fig. S21** SEM images of (a) fresh bare Zn and (b) cycled Zn anode over 800 cycles at 5 A $g^{-1}$.

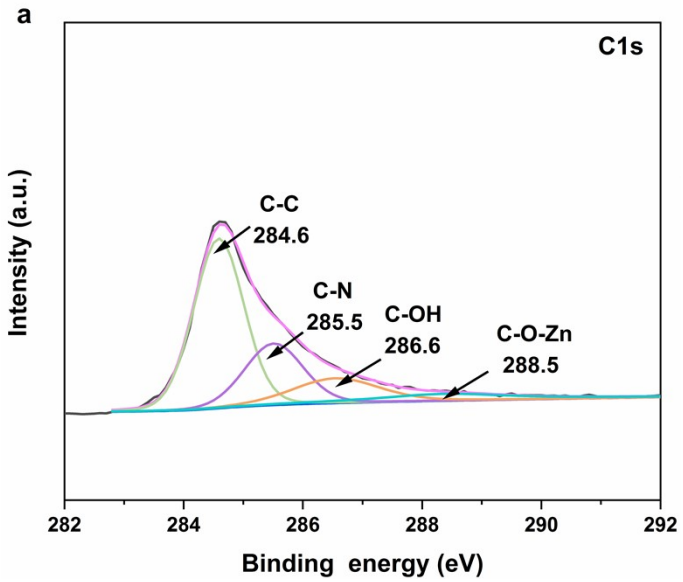


**Fig. S22** The ex situ XPS spectra of C 1s in the fully discharged N-PCNTs cathode.

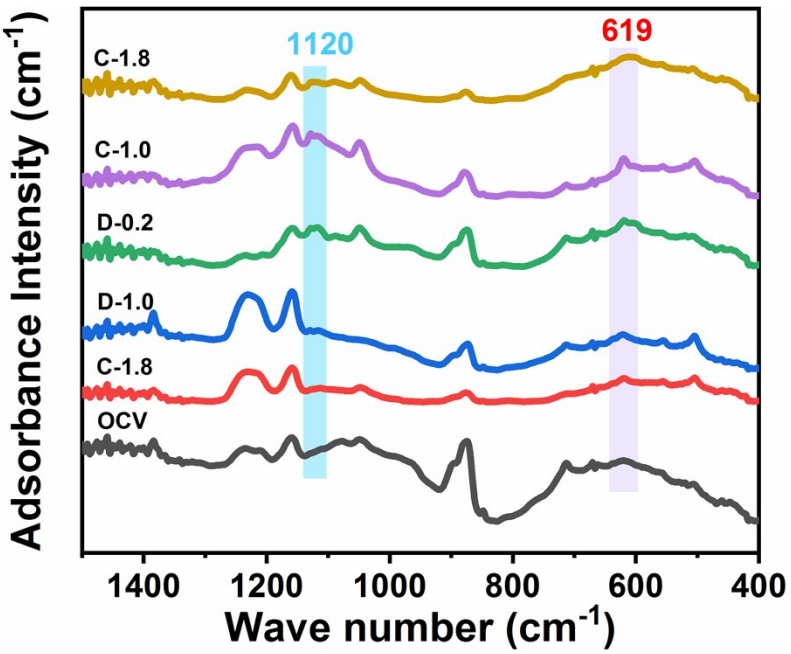


**Fig. S23** The ex situ FTIR spectra of the SN-PCNTs cathode at selected states during charge/discharge processes.

The band at around 619 and 1120 $cm^{-1}$ are assigned to the bending mode of O-S-O and the typical stretching vibration of the $SO_4$ group, respectively, further suggesting the reversible formation/decomposition of $Zn_4SO_4(OH)_6{\cdot}0.5H_2O$ on the SN-PCNTs cathode during the charge/discharge processes.[10, 11]

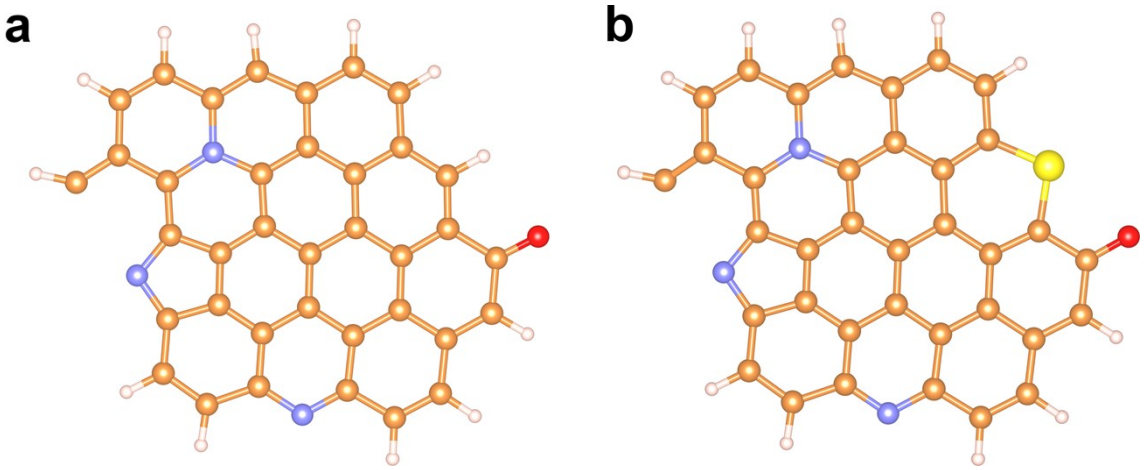


**Fig. S24** The models of (a) N-PCNTs and (b) SN-PCNTs. The brown, blue, yellow, red and pink color indicates C, N, S, O and H atom, respectively.

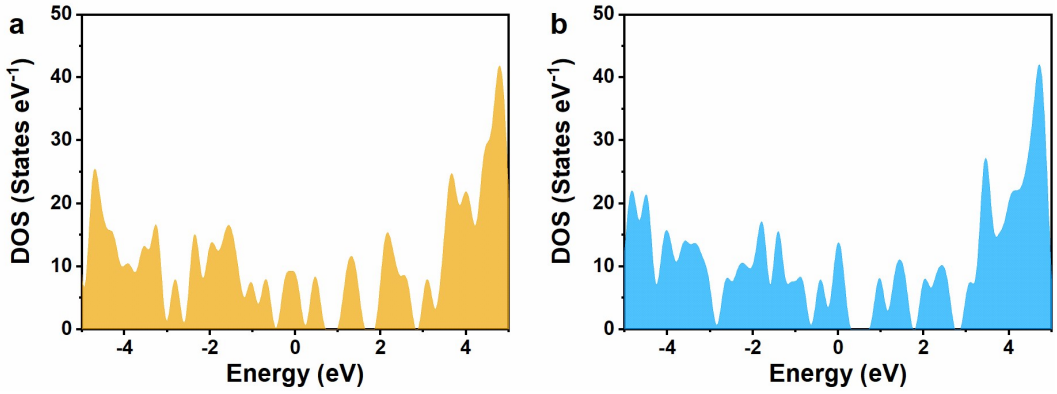


**Fig. S25** Density of states of (a) N-PCNTs and (b) SN-PCNTs after $Zn^{2+}$ adsorption.

**Table S1** Electrochemical performance comparison of the reported ZHCs based on carbon cathodes.

| Materials | Voltage (V) | Capacity (mAh $g^{-1}$) | Energy density (Wh $kg^{-1}$) | Power density (kW $kg^{-1}$) | Cycling stability | Ref. |
|---|---|---|---|---|---|---|
| **SN-PCNTs** | **0.2-1.8** | **152.6/0.2 A $g^{-1}$** | **95.9** | **19.17** | **93.5%/25000 cycles/5 A $g^{-1}$** | **This work** |
| AC | 0.2-1.8 | 121/0.1 A $g^{-1}$ | 84 | 14.9 | 91%/10000 cycles/1 A $g^{-1}$ | 12 |
| AC | 0.2-1.8 | 132/0.1 A $g^{-1}$ | 140.8 | 2.85 | 72%/20000 cycles/4 A $g^{-1}$ | 13 |
| AC | 0.2-1.8 | – | 82.9 | 10 | 98.8%/5000 cycles/1 A $g^{-1}$ | 14 |
| CNPK | 0.2-1.8 | 103.2/0.1 A $g^{-1}$ | 81.1 | 13.366 | 101.8%/10000 cycles/5 A $g^{-1}$ | 15 |
| OPC | 0.2-1.8 | 132.7/0.2 A $g^{-1}$ | 82.36 | 3.76 | 87.6%/10000 cycles/1 A $g^{-1}$ | 16 |
| Ca-900 | 0-1.8 | ~100/0.1 A $g^{-1}$ | 75.22 | 0.879 | 90.8%/4000 cycles/1 A $g^{-1}$ | 17 |
| NPC | 0-1.8 | 136.2/0.3 A $g^{-1}$ | 81.1 | 12.8 | 98.9%/60000 cycles/10 A $g^{-1}$ | 18 |
| LDC | 0.2-1.8 | 127.7/0.5 A $g^{-1}$ | 97.6 | 12.1 | – | 19 |
| AC | 0.2-1.8 | - | 70.4 | 7.6 | - | 2 |
| HBC | 0.2-1.8 | 95.4/0.1 A $g^{-1}$ | – | – | 98%/1000 cycles/1 A $g^{-1}$ | 20 |

**Reference**


1. J. Li, L. Yu, Y. Li, G. Wang, L. Zhao, B. Peng, S. Zeng, L. Shi and G. Zhang, *Nanoscale*, 2021, **13**, 692-699.
2. D. Han, S. Wu, S. Zhang, Y. Deng, C. Cui, L. Zhang, Y. Long, H. Li, Y. Tao, Z. Weng, Q. H. Yang and F. Kang, *Small*, 2020, **16**, 2001736.
3. G. Kresse and J. Hafner, *Phys. Rev. B*, 1993, **47**, 558-561.
4. G. Kresse and J. Furthmüller, *Phys. Rev. B*, 1996, **54**, 11169-11186.
5. G. Kresse and D. Joubert, *Phys. Rev. B*, 1999, **59**, 1758-1775.
6. J. P. Perdew, K. Burke and M. Ernzerhof, *Phys Rev Lett*, 1996, **77**, 3865-3868.
7. H. J. Monkhorst and J. D. Pack, *Phys. Rev. B*, 1976, **13**, 5188-5192.
8. C. P. Ewels and M. Glerup, *J Nanosci Nanotechnol*, 2005, **5**, 1345-1363.
9. J. Ruan, F. Mo, Z. Chen, M. Liu, S. Zheng, R. Wu, F. Fang, Y. Song and D. Sun, *Adv. Energy Mater.*, 2020, **10**, 1904045.
10. D. Zhang, X. Liu, H. Wan, N. Zhang, S. Liang, R. Ma and G. Qiu, *ACS Sustainable Chem. Eng.*, 2017, **5**, 5869-5879.
11. Z. Tie, L. Liu, S. Deng, D. Zhao and Z. Niu, *Angew. Chem., Int. Ed.*, 2020, **59**, 4920-4924.
12. L. Dong, X. Ma, Y. Li, L. Zhao, W. Liu, J. Cheng, C. Xu, B. Li, Q.-H. Yang and F. Kang, *Energy Storage Mater.*, 2018, **13**, 96-102.
13. Z. Wang, J. Huang, Z. Guo, X. Dong, Y. Liu, Y. Wang and Y. Xia, *Joule*, 2019, **3**, 1289-1300.
14. K. Zou, P. Cai, X. Deng, B. Wang, C. Liu, Z. Luo, X. Lou, H. Hou, G. Zou and X. Ji, *Chem. Commun.*, 2021, **57**, 528-531.
15. H. Zhang, Z. Chen, Y. Zhang, Z. Ma, Y. Zhang, L. Bai and L. Sun, *J. Mater. Chem. A*, 2021, **9**, 16565-16574.
16. Y. Zheng, W. Zhao, D. Jia, Y. Liu, L. Cui, D. Wei, R. Zheng and J. Liu, *Chem. Eng. J.*, 2020, **387**, 124161.
17. Y. Zhang, Z. Wang, D. Li, Q. Sun, K. Lai, K. Li, Q. Yuan, X. Liu and L. Ci, *J. Mater. Chem. A*, 2020, **8**, 22874-22885.
18. X. Shi, H. Zhang, S. Zeng, J. Wang, X. Cao, X. Liu and X. Lu, *ACS Materials Lett.*, 2021, **3**, 1291-1299.
19. Y. Lu, Z. Li, Z. Bai, H. Mi, C. Ji, H. Pang, C. Yu and J. Qiu, *Nano Energy*, 2019, **66**, 104132.
20. R. Fei, H. Wang, Q. Wang, R. Qiu, S. Tang, R. Wang, B. He, Y. Gong and H. J. Fan, *Adv. Energy Mater.*, 2020, **10**, 2002741.